CHAPTER VI

PEROXIDATION ACTIVITIES OF HIGHLY DISPERSED Mo-MCM-41 PRODUCED FROM SILATRANE AND MOLYBDENUM GLYCOLATE PRECURSORS

6.1 Abstract

High surface area and dispersion Mo/MCM-41 catalysts were successfully prepared using high purity silatrane and molybdenum glycolate precursors. The precursors were synthesized using the Oxide One Pot Synthesis (OOPS) process. Mo was loaded onto MCM-41 by impregnation before and after heat treatment. After heat treatment, the catalysts were characterized using DRUV, XRD, FTIR, Laser Raman and BET. The %Mo dispersion was as high as 10 mol% or 0.265 g MoO_3/g SiO_2 while the structure of MCM-41 was still retained. Bulk MoO_3 was observed in the case of Mo-loaded onto calcined support of MCM-41(c). Mo loaded uncalcined silicate MCM-41 support showed better catalytic activity during peroxidative reaction.

6.2 Introduction

Molybdena/silica catalysts are of importance in hydrodesulfurization and hydrodenitrogenation processes in petroleum industry [1-3]. High dispersion of supported Mo was reported to exhibit high catalyst activity for not only thermal reactions, such as, hydrogenation [4], dehydrogenation [5], oxidation [6] and metathesis [7], but also photocatalytic reactions, such as, partial oxidation of hydrocarbon. Although incorporation of transition metal into the zeolite framework has received attention as effective and efficient catalysts with high selectivity for various reactions, incorporation of high concentration of large transition metal atom such as Mo and W, within the rigid framework of zeolite is difficult due to the excess strain brought about by the insertion. Contrarily, high dispersion of molybdenum can

be achieved by incorporating it in to the much more flexible framework of MCM-41 [8]. It is worth noting that MCM-41 is a better support for incorporating at least 1.0wt% highly dispersed molybdenum species than amorphous SiO_2 which could only accommodate 0.1wt% of Mo [9].

Recently, Wongkasemjit and coworkers [10-12] have succeeded in synthesizing highly pure metal alkoxides via the "Oxide One Pot Synthesis (OOPS)" process. Owing to hydrolytic stability of those metal alkoxides, correspondingly high surface areas of mixed metal oxides have thus been prepared [13-15]. They also found that for Ti-MCM-41 catalyst in peroxidative reaction of phenol red to catalyze the halogenation of organic substrates, the reaction was facilitated by high surface area and pore diameters of the MCM-41 support [16-17].

In this paper, our aim is to study the use of moisture stable silatrane and molybdenum glycolate precursors to control the dispersion and quantity of molybdenum incorporated onto MCM-41. Photocatalytic activity of synthesized Mo-MCM-41 is investigated, as well.

6.3 Experimental

6.3.1 Materials

Fumed silica (SiO_2) and molybdenum oxide (MoO_3) were purchased from Aldrich Chemical Co. Ethylene glycol ($HOCH_2CH_2OH$), triethanolamine (TEA, $N(CH_2CH_2OH)_3$), potassium bromide (KBr) and hydrogen peroxide (H_2O_2) were purchased from Carlo Erba Reagent. Acetronitrile (CH_3CN) and phenolsulfonephthalein (phenol red) were supplied by Labscan Asia Co. and used as received. Hexadecyltrimethyl ammonium bromide (CTAB) and sodium hydroxide were purchased from Sigma Chemical Co. Hepes buffer solution was obtained from Fluka.

6.3.2 Material Characterization

FTIR spectroscopic analysis was conducted on a Bruker Instrument (EQUINOX55) with a resolution of 4 cm^{-1}. Thermal properties were analyzed using thermogravimetric analysis (TGA) on Du Pont Instrument TGA 2950. The mesoporous product was characterized on a Rigaku X-ray diffractometer at a scanning speed of 2 degree/min using CuKα as source. The working range was 2θ = 1.5-10. Surface area and average pore size were estimated using the BET method on a Quantasorb JR. (Autosorb-1). Laser Raman analysis was conducted using a Horiba HR800 spectrometer. The product was degassed at 250°C for 12 hr prior to analysis. Diffuse reflectance ultraviolet spectroscopy on a Shimazu 2550 spectrometer was used to identify the location and the coordination of molybdenum in hexagonal structure. The reflectance output from the instrument was converted using Kubelka-Munk algorithm. The Si/Al ratio was determined using EDS-SEM on JEOL. The calcination was achieved using a Carbolite furnace (CFS 1200) with a heating rate of 1°C/min.

6.3.3 Synthesis of Silatrane

Wongkasemjit's [18] synthetic method was followed by mixing silicon dioxide and triethanolamine in a ratio of 1:2 in a simple distillation set using ethylene glycol solvent. The reaction was carried out at the boiling point of ethylene glycol under nitrogen atmosphere to remove water as by-product along with ethylene glycol from the system. The reaction was run for 10 hr and the rest of ethylene glycol was removed under vacuum (1.6 Pa) at 110°C. The brownish white solid was washed with acetonitrile for three times to obtain the final white powder product having theoretical ceramic yield of around 19%.

6.3.4 Synthesis of Molybdenum Glycolate

The method of Wongkasemjit was followed [10] by reacting molybdenum oxide with ethylene glycol in a simple distillation set. The reaction was carried out at 150°C for 15 min under nitrogen atmosphere, followed by separating unreacted

MoO_3 from the solution part. The obtained solution was left to crystalline, followed by washing with acetonitrile for three times to obtain white crystal product.

6.3.5 Synthesis of MCM-41

The synthesis followed Wongkasemjit's work [16] by mixing silatrane (0.004 mol) with a solution containing CTAB (0.00112 mol), NaOH (0.001 mol) and TEA (0.014 mol). Water (0.36 mol) was then added with vigorous stirring at 80°C for 3 hr to result in crude product. The resulting crude product was filtered and washed with water to provide white solid product. The synthesized support was divided into 2 parts for directly impregnating molybdenum before and after calcination at 550°C for 3 hr called *"**MCM-41(u)** and **MCM-41(c)**"*, respectively.

6.3.6 Synthesis of Catalysts

Incipient wetness impregnation was used to incorporate Mo onto the MCM-41 support using 3, 5, 7 and 10 mol% molybdenum glycolate precursor. The precursor was dissolved in water and dropped onto the catalyst supports, MCM-41(c) and MCM-41(u). Evaporation of water was carried out at 100°C in the oven for 12 hr, followed by calcination at 550°C. The product obtained was characterized using DRUV, XRD, EDS, FTIR, Laser Raman and BET.

6.3.7 Catalytic Activity Study

The peroxidative bromination test was used to qualitatively study catalyst activity. Mo-MCM-41 (5 mg) was added into a mixture of phenol red (0.2 mM), KBr (0.1 M) and H_2O_2 (10 mM) in 0.1M HEPES buffer having pH 6.5. The mixture was stirred for various times. The formation of 2-[(3,5-dibromo-4-hydroxyphenyl)(3,5-dibromo-4-oxo-2,5cyclohexadienylidene)methyl] benzenesulfonic acid (bromophenol blue) from phenol red was monitored by UV-vis after removing the solid catalyst.

6.4 Results and Discussion

6.4.1 Mo-MCM-41 Synthesis

Long range structural order of Mo loaded MCM-41(u) was shown as small angle diffractogram in Fig.1, indicating a well-resolved pattern of hexagonal mesostructure at 100, 110 and 200 hk0 reflections (where a = b and c = ∞) [19-20]. Amoros *et al* were also successful in synthesizing MCM-41 and its derivatives using silatrane [21-24], and mentioned the use of moisture stable silatrane in controlling both hydrolysis and condensation reactions, thus giving better long range ordering of the structure.

With increasing %Mo loading, the XRD peaks are expected to be broader and lower in intensity due to higher quantity of large molybdenum atoms dispersed, making the structure less uniform and more strained. This result was also observed in other studies [25-26]. However, in our case, even with 10 mol% Mo the XRD pattern of MCM-41 is still retained. Gao *et al* reported the dispersion of MoO_3 onto MCM-41 using thermal treatment process [25], and found that the critical dispersion capacity limit of MoO_3 into MCM-41 is 0.26 g of MoO_3 per g of SiO_2. Loading above this critical limit would completely destroy the mesostructure. In our study, hexagonal mesostructure of MCM-41 is still maintained at molybdenum loading of 0.265 g/g support while in Gao's work the hexagonal pattern was disappeared when Mo loadind over 0.26 g/g. The reason may be that our high surface area and high pore volume offered high amount of silanol groups on the surface of the support, allowing Mo to form Si-O-Mo bridges which caused the distortion of siloxane bond (Si-O-Si) angle [25].

Wide angle XRD was used to confirm the dispersion of Mo onto MCM-41. The molybdenum supported MCM-41(u) showed no characteristic peaks of MoO_3 cluster even when 10mol% of Mo was loaded, verifying the high dispersion of molybdenum on the support. For MCM-41(c), it showed very low intensity of characteristic peaks of bulk MoO_3 (JCPDS 35-609), as illustrated in fig 2. From these results, we can conclude that impregnation of Mo onto uncalcined supports, MCM-41(u), gives better dispersion of molybdenum atom. It may be due to the fact that the

uncalcined support has ability to re-hydrolyze and condense with molybdenum glycolate to form linkages between Mo and silanol groups of the support.

Figure 3 shows the DRUV results of prepared catalysts. Traditionally, absorption band from 230-280 nm was assigned to Mo (T_d) and band from 270-330 nm was assigned to Mo (O_h) [27]. However, Strucky *et al* reported that, when molybdenum was grafted onto MCM-48, the isolated tetrahedral molybdenum species were shifted to higher energies, 216 nm [28]. In our case, all DRUV spectra show the intense band mostly in the form of isolated molybdenum species. A possible mechanism of the formation of isolated metal species using molybdenum glycolate was illustrated in the below schematic.

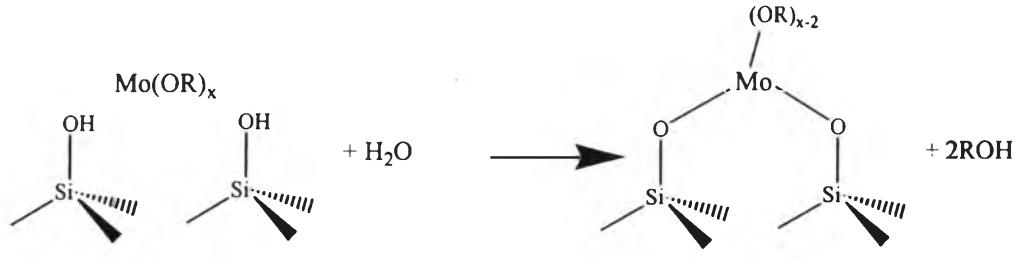

Mo loaded support after calcination, MCM-41(c), gave broader bands and more shoulder at 270-330 nm, corresponding to higher formation of octahedral molybdenum species or higher formation of polymolybdate than Mo loaded support before calcination, MCM-41(u).

Low frequency vibration of supported MoO_3 has been extensively studied by laser Raman spectroscopy. However, Raman has many limitations including thermal decomposition of the sample. FTIR technique, on the other hand, is widely used in the region above 1200 cm^{-1}, but the region below 1200 cm^{-1} also contains useful information about the vibration of heavier atoms as transition-metal bridging to oxygen. Thus, in this work, both FTIR (Figure 4) and laser Raman (Figure 5) techniques were used together to provide complementary data. From previous studies [28-30], there were 3 main intense bands at 927, 970 and 994 cm^{-1}, being characteristics of oxomolybdate species, assigned to Mo-O-Si vibration, terminal M=O group in molybdate phase and MoO_3, respectively. In this work, only 2 bands at 927 and 970 cm^{-1} were clearly observed. The band at 994 cm^{-1} was not clearly seen

indicative of very low content of Mo in the form of MoO_3 species and the interference of intense band of Si-OH group. In contrast, increasing Mo loading, the FTIR result showed an increase in intensity at 927 cm^{-1}, due to the increasing numbers of Mo-O-Si linkages. The band at 994 cm^{-1} of MoO_3 species was still not seen, meaning that molybdenum glycolate tended to form more linkage with the support than with itself. Comparing between Mo-loaded onto MCM-41(u) and MCM-41(c), MCM-41(u) showed higher intensity and well resolved band at 927 cm^{-1}, corresponding to higher degree of Si-O-Mo linkage. The explanation could be stated that Mo was easier to incorporate in uncalcined support due to higher contents of silanol group. After thermal treatment, the concentration of silanol group decreased as a result of dehydroxylation reaction to form siloxane bond.

Raman spectra, fig 5, for MoO_3, shows sharp peaks at 819 and 666 cm^{-1} of Mo-O-Mo bridge, the stretching mode of terminal Mo=O groups at 995 cm^{-1} and wagging mode at 290-280 cm^{-1}[25, 27]. The characteristic peak of bulk MoO_3 was observed only in the sample of MCM-41(c) which is coincident with the FTIR results. For Mo loaded onto MCM-41(u), no Raman peaks were visible for MoO_3, indicating that all loaded Mo were mostly in the form of Mo-O-Si bonds, as confirmed by tetrahedral position in DRUV and high intensity of 927cm^{-1} in FTIR. Our work is in good agreement with Howe and coworkers [29].

Nitrogen adsorption/desorption isotherms of Mo-MCM-41 at various %Mo loading are shown in fig.6. All the isotherms are of type IV classification of IUPAC with five distinct regions, giving sharp inflection with relative pressure > 0.3 representing characteristics of capillary condensation within uniform pores. Filling of the mesopores takes place over a relatively small range of relative pressure, indicative of nearly equal sized pores. A further support for this interpretation is that the desorption curve almost completely coincides with the adsorption isotherm in this pressure range. However, increasing the %Mo up to 10mol%, the inflection becomes less sharp/broader evidence of the destruction of meso-structure, as confirmed by a decrease in intensity of XRD pattern. The BET surface areas are listed in table I. As can be seen, the BET surface areas of the prepared catalysts are high, even for 10 mol% of Mo loading. The pore size decreases with increasing %Mo due to the presence of Mo oxide in the channels of the support. High surface areas were also

observed in our previous studies on MCM-41 and Ti-MCM-41 syntheses using silatrane and titanium glycolate precursor [16]. The precursors are more inert toward hydrolysis than TEOS or other commercially available metal alkoxides, thus, there is a good balance between hydrolysis and condensation was able to achieve, giving enough time for silica molecules to arrange with a high degree of ordering without the collapse of the framework.

6.4.2 Catalytic Activity Testing

Because of the large surface area and monodispersed pore size, Mo loaded MCM-41 offers more opportunity to create reaction sites and molecular confinement which may permit more selective products to form. It was reported to biomimic functions of vanadium [31], zirconium [32], titanium [17], molybdenum and tungsten [28]. This behavior was reported to be a close analogue to the role of vanadium peroxidase enzyme (V-BrPO) which performs this function in the marine environment to produce brominated natural products with pharmacological activity, possibly preventing the host organism from being infected or eaten [17, 33-34]. Thus, in this work Mo-MCM-41 was tested for the catalytic halogenation reaction as discovered in biocatalytic process.

Figure 7 shows that phenol red was transformed when reacted with Mo-MCM-41 catalyst in the presence of H_2O_2 from λ_{max}= 450 nm into λ_{max}= 589 nm, corresponding to bromophenol blue [35]. The change is similar to those reported using Ti-MCM-41 catalyst [16-17]. In fact, the role of H_2O_2 in the system is to activate the metal peroxo complex which is an effective oxidant in solution [36]. Figure 8 shows that the rate of oxidation with hydrogen peroxide alone is much slower when compared to the reaction rates in the presence of solid catalyst. In the presence of the solid catalyst, the absorbtion at λ_{max}= 589 nm increased rapidly while only a slight increase was observed at 589 nm when only H_2O_2 was added. As the reaction time increased, the absorbance at λ_{max}= 589 nm increased, indicating that more bromination of phenol red took place to form bromophenol blue. Fig 9 also illustrates the activity comparison of Mo-MCM-41(c) and Mo-MCM-41(u), showing

the lower activity of Mo-MCM-41(c). This is most likely due to the higher activity and concentration of tetrahedrally coordinate form of molybdenum in MCM-41 (u). It is known that the rate limiting step of this reaction is the cleavage of O-O bonds, and the weaker O-O bonds are found in the active compounds due to the electron-withdrawing effect of the central metal. The bond polarity then promotes heterolytic O-O bond cleavage upon nucleophilic attack, favoring a non-radical pathway for oxidative bromination via a reactive OBr^- species. [28]

6.5 Conclusions

High dispersion of molybdenum onto MCM-41 supports was successfully carried out using high purity silatrane and molybdenum glycolate precursors. The structure of hexagonal array is still retained even for 10 mol% of Mo or ≈0.265 g/g of SiO_2. The surface area of Mo-MCM-41 is in excess of 1600 m^2/g. Loading onto uncalcined MCM-41 resulted in higher metal dispersion and higher activity.

6.6 Acknowledgements

This research work is supported by the Postgraduate Education and Research Program in Petroleum and Petrochemical Technology (ADB) Fund, Ratchadapisake Sompote Fund, Chulalongkorn University and the Thailand Research Fund (TRF).

6.7 References

1. Reddy KM, Wei B, Song C. *Catal. Today.* 1998; 43: 261.
2. Song C, Reddy KM, *Appl. Catal.* 1999; 176: 1.
3. Cordero RL, Agudo AL. *Appl. Catal. A.* 2000; 202: 23.
4. Halachev T, Nava R, Dimitrov L. *Appl. Catal. A.* 1998; 169: 111.
5. Heracleous E, Lemonidou AA, Lercher JA. *Appl. Catal. A.* 2004; 264: 73.
6. Parvulescu V, Su BL. *Catal. Today.* 2001; 69: 315.

7. Handzlik J, Stoch J, Ogonowski J, Mikolajczyk M. *J. Mol. Catal. A.* 2000; 157: 237.
8. Matsaya M, Anpo M. *J. Photochem. Photobio. C: Photochem. Rev.* 2003; 3: 225.
9. Louis C, Che M, Anpo M. *J. Catal.* 1993; 141: 453.
10. Sutara S, Gulari E and Wongkasemjit, S. *Proceeding of the International Conference on Smart Material (SmartMat-'04)* December 1-3, 2004. Chiang Mai, Thailand.
11. Ksapabutr, B., Gulari, E. and Wongkasemjit, S., *Materials Chemistry and Physics* 2004, 83/1, 34-42.
12. Opornsawad, Y., Ksapabutr, B., Wongkasemjit, S. and Laine, R., *Eur. Polym. J.* 2001, 37/9, 1877-1885.
13. Ksapabutr, B., Gulari E. and Wongkasemjit, S., *Powder Technology* 2004, 148/1 pp. 11-14.
14. Ksapabutr, B., Gulari, E. and Wongkasemjit, S., *Colloids and Surface A* 2004, 233, 145-153.
15. Phonthammachai, N., Chairassameewong, T., Gulari, E., Jamieson, A.M. and Wongkasemjit, S., *Mesoporous and Microporous. Mater.* 2003, 66/2-3, pp. 261-271.
16. Thanabodeekij N, Tanglumlert W, Gulari E, Wongkaswmjit S. *Appl. Organo. Metal.* 2005 (In Press).
17. Walker JV, Morey M, Carlsson H, Davidson A, Stucky DG, Bulter A. *J. Am. Chem. Soc.* 1997; 119: 6921.
18. Charoenpinijkarn W, Sawankruhasn M, Kesapabutr B, Wongkasemjit S, Jamieson AM. *Eur. Polym. J.* 2001; 37: 1441.
19. Shan Z, Jansen JC, Marchese L, Maschmeyer TH *Micropor. Mesopor. Mater.* 2001; 48: 181.
20. Haskouri JE, Cabrera S, Gutierrez M, Beltran-Porter A, Beltran-Porter D, Marcos MD, Amoros P. *Chem. Commun.* 2001; 7: 1437.
21. Haskouri JE, Cabrera S, Caldes M, Alamo J, Beltran-Porter A, Marcos MD, Amoros P, Beltran-Porter D. *Int. J. Inorg. Mater.* 2001; 3: 1157.
22. Haskouri JE, Cabrera S, Caldes M, Alamo J, Beltran-Porter A, Marcos MD, Amoros Beltran-Porter D. *Chem. Mater.* 2002; 14: 2637.

23. Cabrera S, Haskouri JE, Carmen G, Julio L, Beltran-Porter A, Beltran-Porter D,Marcos M D, Amoros P. *Solid State Science* 2000; 2: 405.
24. Haskouri JE, Cabrera S, Gutierrez M, Beltran-Porter A, Beltran-Porter D, Marcos MD, Amoros P. *New J. Chem.* 2002; **26**: 1093.
25. Li Z, Gao L, Zheng S. *Appl. Catal. A.* 2002; **236**: 163.
26. Piquemal JY, Mnoli JM, Beaunier P, Ensuque A, Tougne P, Legrand AP, Bregeault JM. *Micropor. Mesopor. Mater.* 1999; **29**: 291
27. Williams CC, Ekerdt JG, Jehng JM, Hardcastle FD, Turek AM, Wachs IE. *J. Phys. Chem.* 1991; **95**: 8781.
28. Morey MS, Bryan JD, Schwarz S, Stucky D. *Chem. Mater.* 2000; **12**: 3435.
29. Seyedmonir SR, Abdo S, Howe RF. *J. Phys. Chem.* 1982; **86**: 1233.
30. El Shafei GMS, Mokhtar MM. *Colloids Surf. A.* 1995; **94**: 267.
31. Clague MJ, Bulter A. *J. Am. Chem. Soc.* 1995; **117**: 3475.
32. Morey MS, Schwarz S, Froba M, Stucky GD. *J. Phys. Chem. B.* 1999; **102**: 2037.
33. Meister GE, Bulter A. *Inorg. Chem.* 1994; **33**: 3269
34. .Colpas GJ, Hamstra BJ, Kampf JW, Percoraro VL. *J. Am. Chem. Soc.* 1996; **118**: 3469.
35. Sozedjak HS, Bulter A. *Inorg. Chem.* 1990; **29**: 5015.
36. Ghiron AF, Thompson RC. *Inorg. Chem.* 1990; **29**: 4457.

Table 6.1 BET results of catalysts synthesized at different Mo loadings

%Mo	Surface Area (m^2/g)	Pore Volume (cc/g)	Pore Size (nm)
MCM-41 (u)			
3	1680	1.28	3.04
5	1533	1.13	2.95
7	1471	1.25	3.16
10	1394	1.00	2.61
MCM-41 (c)			
3	1600	1.31	3.08
5	1562	1.2	2.97
7	1478	1015	2.77
10	1377	1.05	2.61

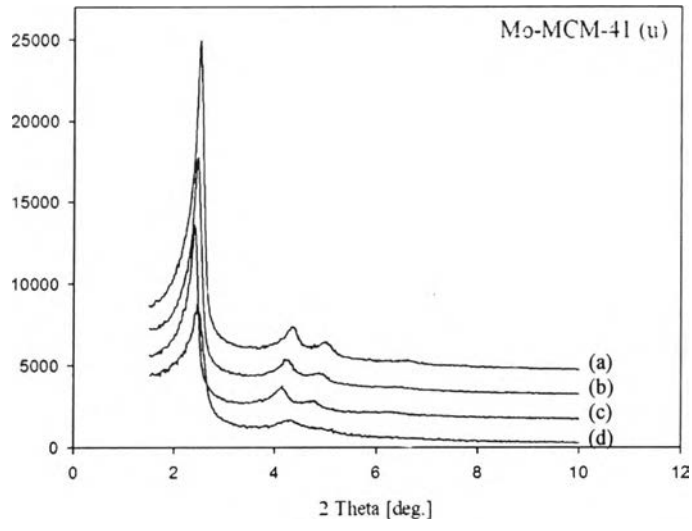

Figure 6.1 XRD spectra of MCM-41(u) containing various %Mo loading; **(a)** 3%, **(b)** 5%, **(c)** 7% and **(d)** 10%Mo.

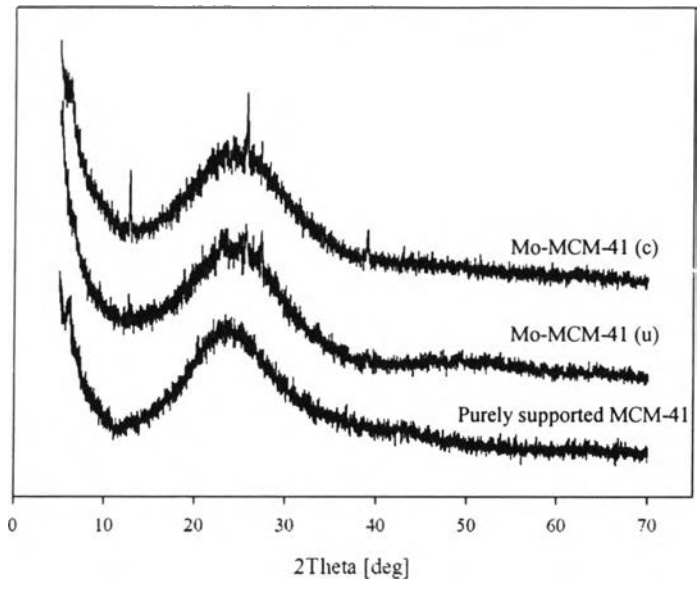

Figure 6.2 Wide angle XRD spectra of pure support MCM-41, 10 mol% Mo-MCM-41(u) and 10 mol% Mo-MCM-41(c).

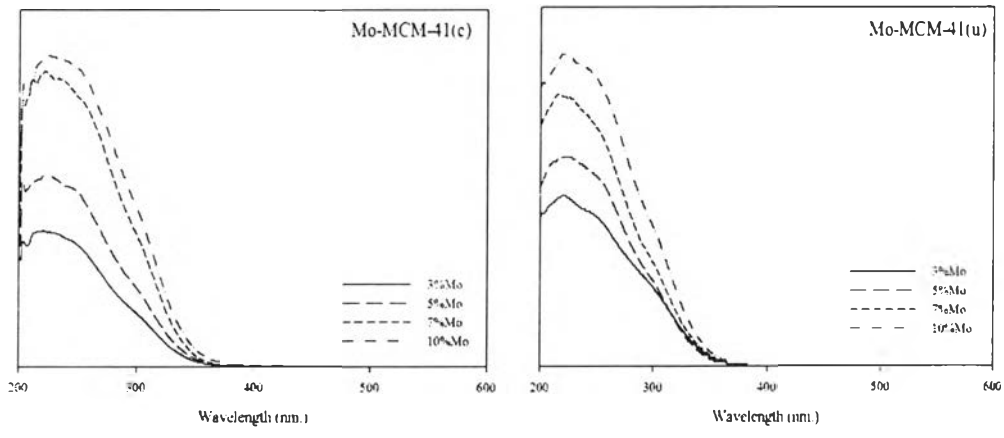

Figure 6.3 DRUV spectra of Mo-MCM-41(u) and Mo-MCM-41(c) at various %Mo loadings.

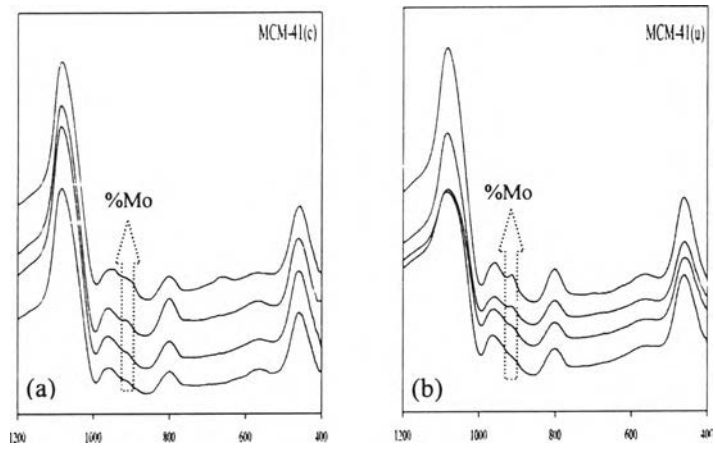

Figure 6.4 Comparison of FTIR spectra of 3%, 5%, 7% and 10% Mo loaded onto; **(a)** MCM-41(c) and **(b)** MCM-41(u).

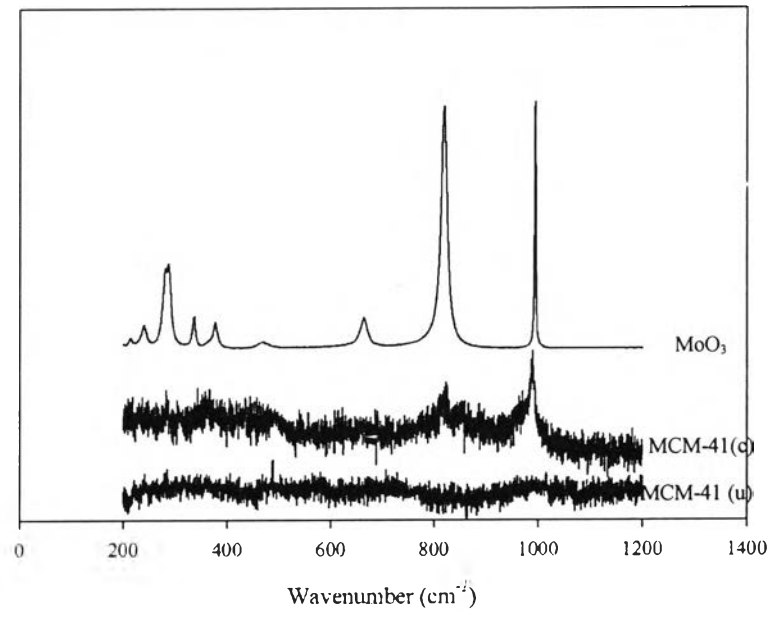

Figure 6.5 Raman spectra of MoO_3 comparing to 10 mol% Mo-MCM-41(u) and 10 mol% Mo-MCM-41(c).

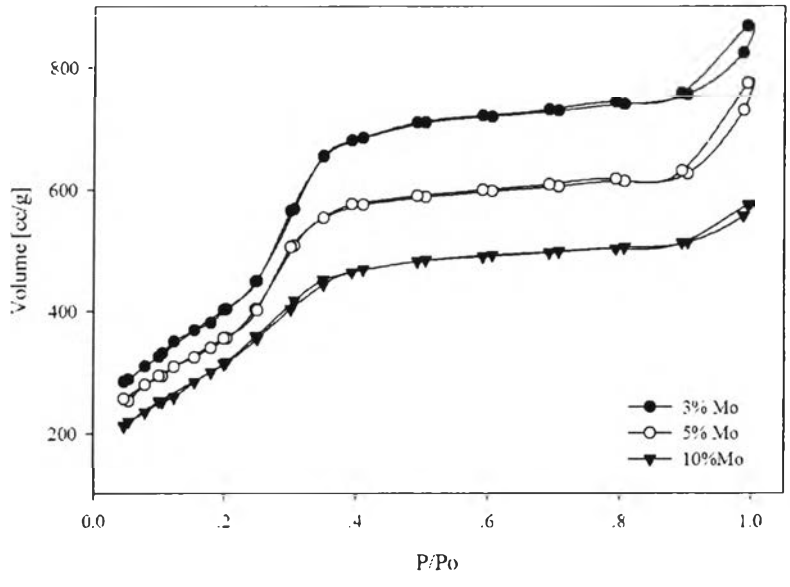

Figure 6.6 Comparison of N_2 adsorption isotherm of Mo-MCM-41 at various % Mo loadings.

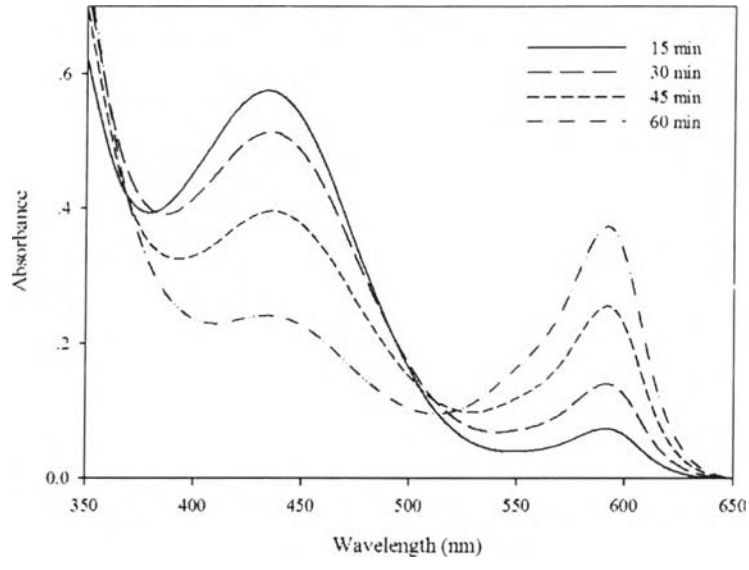

Figure 6.7 UV-vis absorption spectra of solutions peroxidatively brominated phenol sulfone phthalein (phenol red) catalyzed by Mo-MCM-41 for 15, 30, 45 and 60 min.

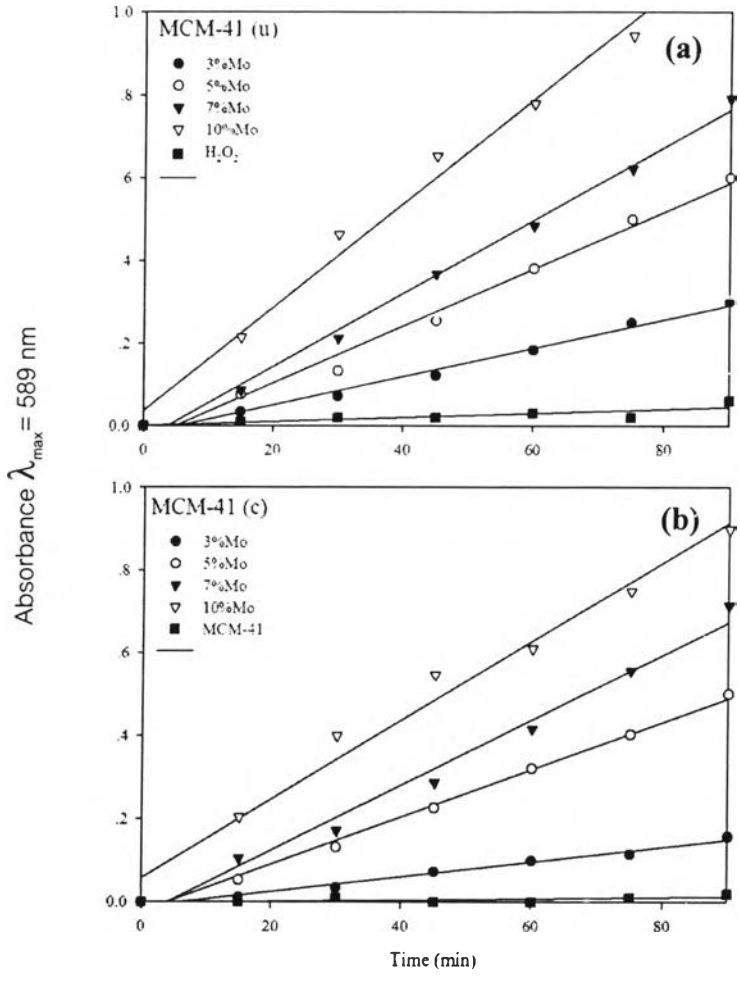

Figure 6.8 Comparison of the peroxidative bromination reaction at various %Mo loadings using; a). MCM-41(u) and b) MCM-41(c).

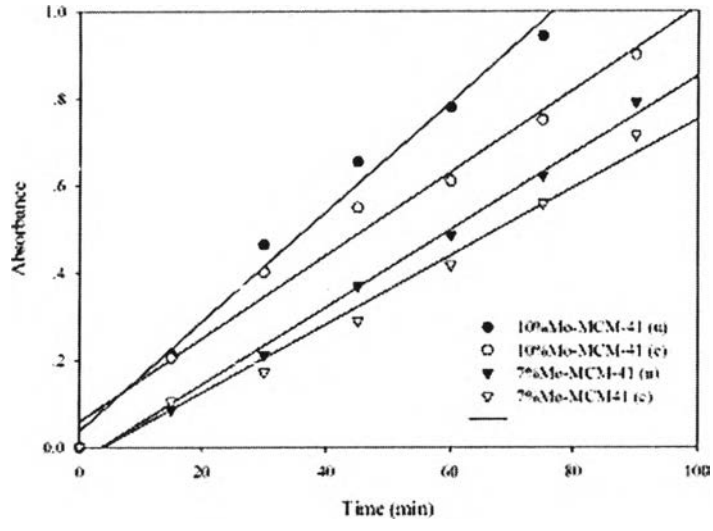

Figure 6.9 Comparison of catalyst activity between Mo loaded onto uncalcined and calcined MCM-41.